Journal of Applied Physics

Enhancing optical transmission of multilayer composites using interfacial nanostructures

Cite as: J. Appl. Phys. **126**, 063101 (2019); https://doi.org/10.1063/1.5097832
Submitted: 28 March 2019 . Accepted: 15 July 2019 . Published Online: 08 August 2019

Yi-An Chen, Sharan V. Naidu, Zhiren Luo, and Chih-Hao Chang

Journal of Applied Physics ARTICLE scitation.org/journal/jap

Enhancing optical transmission of multilayer composites using interfacial nanostructures

Cite as: J. Appl. Phys. **126**, 063101 (2019); doi: 10.1063/1.5097832
Submitted: 28 March 2019 · Accepted: 15 July 2019 ·
Published Online: 8 August 2019

Yi-An Chen, Sharan V. Naidu, Zhiren Luo, and Chih-Hao Chang[a)]

AFFILIATIONS

Department of Mechanical and Aerospace Engineering, North Carolina State University, Raleigh, North Carolina 27695, USA

[a)]**Author to whom correspondence should be addressed:** chichang@ncsu.edu

ABSTRACT

We demonstrate the suppression of light reflections at solid-solid interfaces in multilayer thin and thick films using interfacial nanostructures. The embedded nanostructures have subwavelength features and function as a gradient-index medium to eliminate Fresnel losses induced by refractive index mismatch between dissimilar materials. Suppressing the interfacial reflection can reduce interference effects in thin films, and the transmittance measurement of a polymer on a silica substrate demonstrates a two-fold decrease in interference fringe contrast. A thick multilayer composite consisting of three fused silica and two polymer layers has also been fabricated and demonstrates the enhancement of optical transmission up to 30% at high incident angles. The effects of the interfacial structure geometry are examined by theoretical models based on rigorous coupled-wave analysis methods. The experimental results agree well with simulation models, which predicts that further improvements can be achieved using the optimized tapered profile. This work indicates that interfacial nanostructures can improve the broadband and wide-angle response of multilayers and can find applications in thin-film optics, optoelectronic devices, and composite windows.

INTRODUCTION

In recent years, bioinspired nanostructures have drawn increasing interest because of their novel physical behaviors. An example is the antireflection (AR) nanostructures inspired by the moth eye, which can reduce light reflection on material surfaces.[1–19] The surface reflection can be attributed to a refractive index mismatch at the air-solid interface, which causes Fresnel reflection losses[4,5,10] and reduces transmission. The moth-eye structures serve as a gradient-index medium where its effective index bridges the index mismatch.[1–17] Such an effect operates over a broad wavelength band and a wide viewing angle, which is advantageous over the traditional AR coating.[17,18] Some methods have been demonstrated, for example, engineered surfaces can suppress surface reflections by using electron-beam,[5,9] interference lithography (IL),[4,12,20] colloidal assembly,[21,22] maskless reactive ion etching,[23] and random nanostructures.[24] Another way to achieve a gradient-index AR medium is the oblique-angle deposition of single and multilayer films with varying porosity.[10,25,26] Beyond reducing reflection, nanostructures can also be tuned to enhance the surface absorptivity.[19] These advances have many applications in photonics and optoelectronics devices, such as optical microresonators[27] and light-emitting diodes.[28] These advances can also enable anti-glare, self-cleaning windows,[12] improve the device performance of solar cells,[29–32] and enhance light extraction in solid-state lighting.[33]

While most existing work on AR nanostructures has been focused on material surfaces, Fresnel losses can also occur between two solid materials. This is especially important in multilayer thin films, where multiple interfacial reflections must be considered. Under coherent illumination, such reflections can interfere and induce iridescent effects. This can lead to wavelength and angle-dependent properties, which is undesirable in broadband optical element and devices. This optical effect can be observed in nacre, which is constructed from alternating microscale laminates of stiff and soft materials.[34–37] While most research has been focused on the mechanical properties of nacre such as fracture toughness and strength, their optical properties are often overlooked. Due to the difference in refractive indices, reflection losses between the layers interfere and give rise to the iridescent appearance. While the brilliant color is visually pleasing, it leads to undesirable tinted appearance when the layered architecture is used for transparent substrates. Therefore, the ability to reduce interfacial reflection losses and interference effect is critical for applications in next-generation transparent armor.

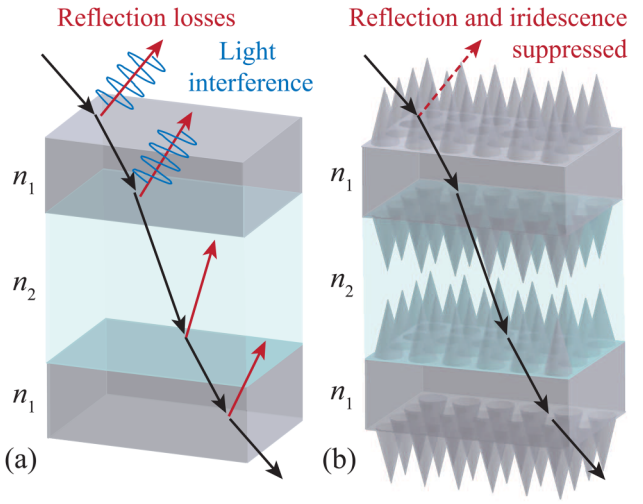

FIG. 1. Schematic of (a) Fresnel losses and light interference in multilayer films with alternating materials with planar interfaces. (b) The reflection and iridescence can be suppressed using interfacial nanostructures.

In our prior work, we demonstrated that the interfacial reflection between a polymer film and a silicon substrate can be suppressed using nanostructures by studying the reflectance spectra.[38] However, the previous study focused on a single interface, and the more complex phenomenon of reflections from multiple interfaces has not been examined. That work also only examined the reflectance spectra, and the question of how the suppression of interfacial reflection affects the broadband transmission remains unanswered. This is especially important when considering that reducing light reflection does not necessarily lead to enhanced transmission, since the specular transmitted order can have losses due to light scattering from fabrication defects in the multilayer interfaces. These effects are illustrated in Fig. 1(a), where reflected orders at each interface can interfere. These losses may be mitigated by introducing tapered nanostructures at the interfaces, as illustrated in Fig. 1(b). The structures emulate as an effective medium with continuously changing index and bridge the neighboring refractive indices. These interfacial nanostructures can reduce the reflections at the interfaces, thereby suppressing iridescent effects induced by interference and increasing light transmission.

In this work, we report the experimental demonstration of interfacial nanostructures, as inspired by both nacre and moth eye, in multilayer thin and thick films to suppress interference effects and enhance broadband transmission. The structures are fabricated on fused silica substrates, serving as a template to create a nanostructured interface by infiltration using different polymer types and thicknesses. A substrate bonding process is used to stack and assemble multiple double-side patterned fused silica substrates, and a thick multilayer composite material consisting of three silica and two polymer layers have been successfully fabricated. The wide-angle and broadband optical performance of these structures was characterized and demonstrates suppressed iridescence and enhanced transmission. The experimental data agree well with constructed simulation models based on rigorous coupled-wave analysis (RCWA) methods.[39,40] The results demonstrate that interfacial nanostructures are an effective method to mitigate wavelength and angle-dependent behavior and enhance broadband transmission in multilayer devices and composite materials.

DESIGN OF INTERFACIAL NANOSTRUCTURES

The optical effects of the interfacial nanostructures between polymer ($n_{poly} = 1.7$) and fused silica ($n_{fs} = 1.45$) are first examined using RCWA models. The polymer and silica are assumed to be semi-infinite media to study the reflection efficiency at the interface. Here, the interfacial nanostructures with a linear taper profile is approximated by discrete 2D gratings with a square lattice and varying duty cycles from 0 to 1. The simulated total reflection efficiencies (R_T) are plotted in log scale vs the nanostructure height and period, as shown in Fig. 2. Note that the total reflection efficiency can include reflected diffracted orders for structures with larger periods. Here, the x-axis and y-axis are normalized nanostructure period (Λ/λ) and height (H/λ), respectively.

The reflection efficiency of a planar polymer-to-silica interface is 0.63% (−2.2 in log scale) at normal incidence, corresponding to $H = 0$ in Fig. 2(a). However, for structure height $H = 2\lambda$ and period $\Lambda = 0.5\lambda$, the reflection efficiency can be decreased to 0.0021% (−4.7 in a log scale). In this case, the interfacial nanostructures reduce the reflection loss by a factor of 300. For slightly shorter structures $H = 0.6\lambda$ with the same period, which has been experimentally demonstrated in this work, the reflection efficiency can be reduced to 0.027% (−3.6 in log scale), roughly a 23-fold improvement over a planar interface. For larger incident angles $\theta_i = 30°$, the reflection efficiency of the planar polymer-to-silica interface is slightly higher at 1.26% (−1.9 in log scale), as shown in Fig. 2(b). The reflection efficiency can be reduced to 0.15% (−2.8 in log scale) for structure height $H = 0.6\lambda$ and period $\Lambda = 0.5\lambda$. The reflection efficiency can be further eliminated to 0.030% (−3.5 in log scale) for nanostructure height $H = 2\lambda$ with the same period. Note that while the reflection losses at a single interface between polymer and silica are generally low, they can be compounded for multiple layers. In addition, the reflection losses would be significantly higher for interfaces with higher index contrast, as discussed later in this work.

It can be observed that the AR effect is stronger for taller interfacial nanostructures, which is expected since this creates a medium with lower index gradient. For a larger nanostructure period, the reflection efficiency increases and results in intensity oscillation. This can be attributed to diffraction orders being no longer evanescent, as marked by the dashed line, resulting in the interfacial nanostructures not in subwavelength operation. The first-order diffraction becomes a propagating mode when the structure period is around $\Lambda = 0.6\lambda$ and $\Lambda = 0.4\lambda$ for incident angles $\theta_i = 0°$ and 30°, respectively. It is also interesting to note that while the structure period has to be subwavelength, having a much smaller period does not greatly reduce reflection losses. The same can be said for structure height, which results in lower reflection but the improvement is incremental. Based on this analysis, we focus on nanostructure with 250 nm period and 400 nm height,

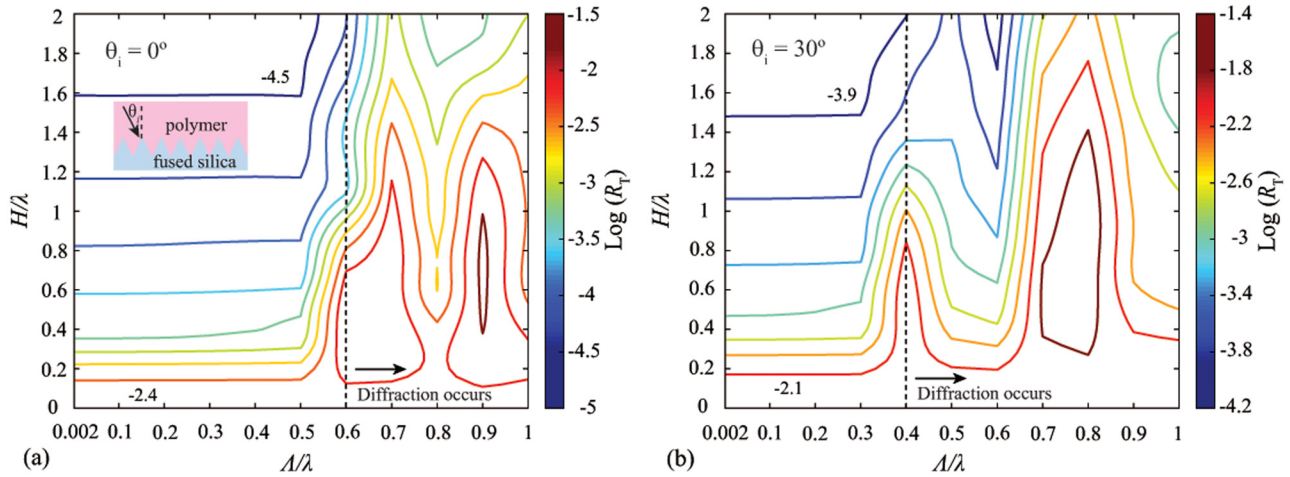

FIG. 2. Simulated 2D contour plots of total reflection efficiency (R_T) at a polymer-to-silica interface ($n_{poly} = 1.7$ and $n_{fs} = 1.45$) using log scale. The reflection is plotted vs normalized structure height and period at incident angles of (a) $\theta_i = 0°$ and (b) $\theta_i = 30°$.

which is expected to exhibit a strong interfacial AR effect in the visible spectrum.

FABRICATION METHOD AND MATERIALS

The proposed interfacial nanostructures are demonstrated in a composite multilayer with alternating polymer and fused silica layers. The structures are patterned using a combination of interference lithography (IL), reactive ion etching (RIE), and substrate stacking, as shown in Fig. 3. First, a fused silica substrate is spin coated with 13 nm antireflection coating (ARC i-con-7, Brewer Science) and 250 nm photoresist (PFI-88A2, Sumitomo), as shown in Fig. 3(a). The ARC film is used to reduce the reflection from the substrate during lithography. A two-dimensional (2D) pillar array is then patterned in the photoresist using two orthogonal exposures in a Lloyd's mirror IL setup[12,41] as illustrated in Fig. 3(b). The structure has 250 nm period. The pattern is then transferred to the underlying fused silica substrate using O_2 and CHF_3 reactive ion etching (RIE). The photoresist mask is also etched during the process, yielding the tapered profile as illustrated in Fig. 3(c). After spin coating a protective polymer film (ProTEK B3-25, Brewer Science) on the front-side nanostructures, the same process is then repeated to pattern the backside of the fused silica substrate, as shown in Fig. 3(d). The ProTek film can be removed in a solvent solution (ProTEK Remover 100, Brewer Science) followed by O_2 plasma etching. This results in a fused silica substrate with subwavelength AR structures patterned on both sides. The double-side patterned fused silica substrates can then be bonded using a UV-curable epoxy (NOA 170, Norland Optical Adhesive), as depicted in Fig. 3(e). The sample is cured in UV light with low

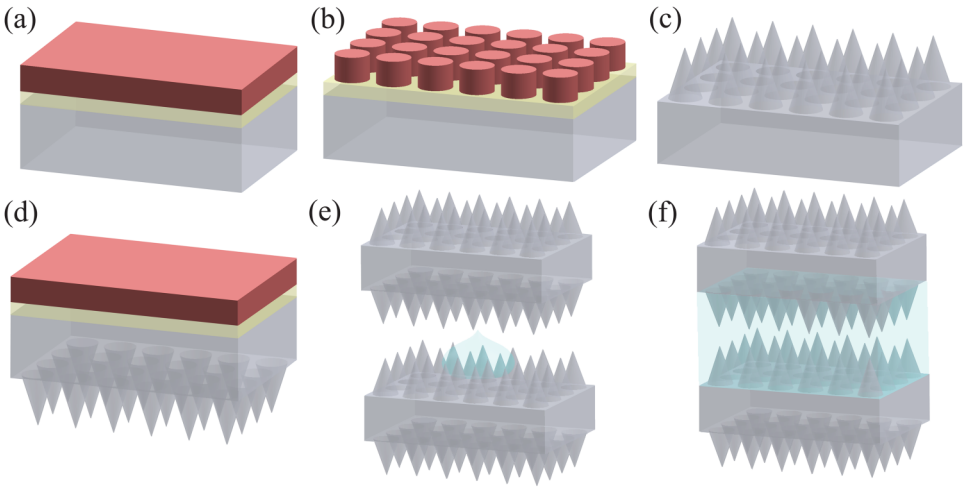

FIG. 3. Schematic of fabrication process. (a) Spin coat ARC and photoresist. (b) Pattern 2D pillar array in photoresist using IL. (c) Etch pattern into fused silica substrate using RIE. (d) Spin coat ARC and photoresist on back surface. (e) Bound double-side patterned fused silica samples using NOA. (f) Fused silica/polymer composite with interfacial nanostructures.

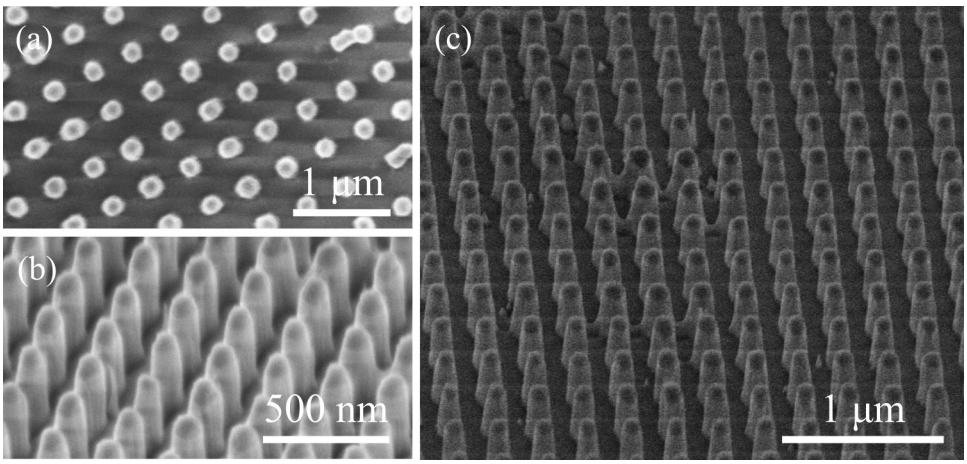

FIG. 4. SEM images of fabricated samples. (a) Top-view image of 2D pillar array in photoresist, (b)–(c) side-view images of 2D taper nanostructures etched into fused silica substrate.

intensity over an hour to reduce bubble formation. The thickness of the epoxy is typically on the order of 0.1 mm. This process can be repeated to construct a thick multilayer silica/polymer composite material with nanostructures embedded at each interface, as shown in Fig. 3(f). Three fused silica substrates, each 0.5 mm thick, have been bonded to yield a silica-polymer-silica-polymer-silica composite. Note that each layer in the composite material is relatively thick compared to the coherent length of ambient light or broadband lamps, meaning that no interference is expected so that the transmission enhancement can be better quantified.

This fabrication process was also used to pattern a thin single-layer polymer sample to examine the effect of thin-film interference on the broadband transmittance. These samples consist of tapered nanostructures patterned on the front side of the fused silica substrate, as illustrated in Fig. 3(c). A thin layer of photoresist (Sumitomo PFI-88) of around 750 nm thickness is then spin coated on the top of fused silica nanostructures. The backside of the substrate is polished but not patterned. These samples, therefore, consist of a nanostructured polymer-silica interface, while the top polymer and bottom fused silica surfaces are planar. Here, the film thickness is less than the coherent length of the spectrophotometer light source, allowing the study of interfacial reflection by quantifying the thin-film interference effects. Note that these samples serve a different purpose to the thick multilayer samples described in the previous paragraph, which consists of tapered nanostructures on both sides for transmission characterization.

The scanning electron microscope (SEM) images of the fabricated nanostructures on the front fused silica substrate are shown in Fig. 4. The top view of a 2D pillar array in photoresist after IL exposure is shown in Fig. 4(a), indicating periodic order in a square lattice. A few photoresist structure collapses can be seen. The side-view SEMs of AR nanostructures etched into the fused silica substrate are shown in Figs. 4(b) and 4(c). The conic profile of the structure can be observed in the higher magnification image shown in Fig. 4(b). The large-area uniformity is illustrated in Fig. 4(c), with some defects due to the residual connection between the structures. Some nanoscale spikes can also be observed and can be attributed to the redeposition of the volatile species during RIE. These results illustrate that the AR nanostructures are well arranged with 250 nm period and around 400 nm height, as desired. Few defects as a result of collapsed resist and surface roughness can be observed. The SEM images of the backside structures indicate a similar structure geometry and quality.

The optical properties of the thin and thick multilayer stacks with interfacial nanostructures are modeled using RCWA, where the tapered nanostructures are approximated by discrete 2D gratings with varying duty cycles. The RCWA model is based on alternating fused silica ($n_{fs} = 1.45$) and polymer ($n_{poly} = 1.70$) layers periodic along both x and y directions. The nanostructures model is approximated as a square lattice with a period of 250 nm. Theoretical models for three types of structures at the interface have been constructed to validate experimental results and evaluate the effectiveness of the interfacial nanostructures. The first is a planar model consisting of continuous polymer film on fused silica substrate layers with no nanostructures. The second describes the fabricated samples with the nanostructured interface. The structure geometry and profile are obtained from the SEM images to accurately simulate the fabricated structure shape. The modeled structure has 400 nm height and 0–0.6 duty cycle. Note that the fabricated structure height and profile have not been optimized for AR performance, and taller structures with 700–800 nm height with more effective tapered profile can be achieved using different etching masks.[10] The third model consists of theoretical structures with 750 nm height and a linear tapered profile from 0 to 1 duty cycle, which describes the performance that can be obtained for a more optimized structure geometry.

RESULTS AND DISCUSSION

The fused silica substrate with a photoresist film was first characterized to study the thin-film interference effects. The thickness of the photoresist layer is around 750 nm, which can be considered a thin film. The broadband transmittance of the thin-film samples with planar and nanostructured interfaces was measured using a UV-visible-NIR spectrophotometer (Cary 5000, Agilent Co.), as shown in Fig. 5. The transmittance measurements from

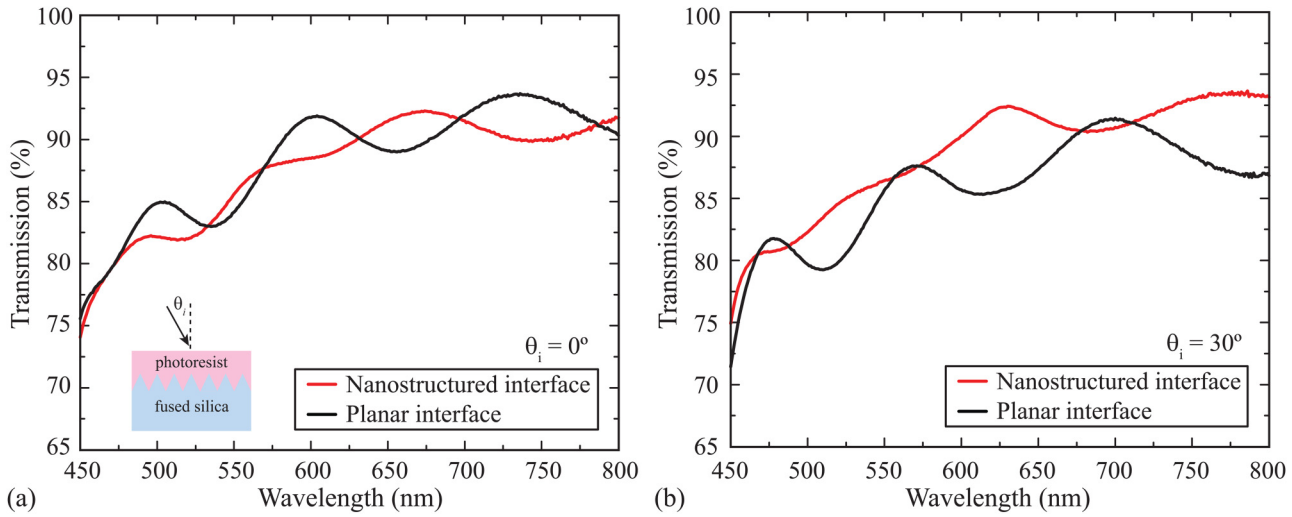

FIG. 5. Broadband measurement data for thin polymer film on fused silica substrates with nanostructured and planar interfaces at incident angles (a) $\theta_i = 0°$ and (b) $\theta_i = 30°$. The film is a layer of photoresist with 750 nm thickness.

450 to 800 nm wavelength for incident angles $\theta_i = 0°$ and 30° are shown in Figs. 5(a) and 5(b), respectively. Intensity oscillations can be observed in all of the measurements, which is a characteristic of interference effects. This is due to reflections from the polymer surface and the polymer-silica interface, which leads to two-beam interference. At incident angle $\theta_i = 0°$, the transmission enhancement for the nanostructured interface is not obvious, as shown in Fig. 5(a). However, the intensity oscillation is reduced. This can be attributed to the reduction of reflection at the polymer-silica interface by the nanostructures, thereby suppressing interference effects. The transmittance measurement for incident angle $\theta_i = 30°$ shows an average of 5% transmission enhancement for the sample with the interfacial nanostructures, as shown in Fig. 5(b). It can also be observed that the intensity oscillation has also been reduced. These results indicate that the sample with the nanostructured interface has higher light transmission and less intensity oscillation due to interference effects.

The interference contrast, or the ratio of the sinusoidal intensity amplitude to the average intensity, can be calculated to quantify the suppression of the thin-film interference effects. The contrast describes the degree of interference for the reflected orders and approaches 0 as the interfacial reflection is suppressed.[38] The contrast values are determined by first fitting the broadband transmittance data using a second order polynomial to estimate the average intensity. The difference between the data and the average intensity can then be calculated to approximate the sinusoidal intensity amplitudes. The contrast of the experimental data can then be defined as the ratio of the amplitude to the average intensity. We focus on the 450–750 nm range, since the sinusoids are not well defined at the long wavelength limit. The calculated contrast values for the samples with and without interfacial nanostructures are plotted in Fig. 6. Since there are multiple maxima and minima, the highest contrast value is plotted and the error bar represents the standard deviation of the calculated values. The theoretical contrast values predicted using RCWA are also plotted. For the nanostructured interface samples, the structure profile was estimated from the SEM images. The planar samples were modeled as a semi-infinite silica substrate with a thin homogeneous polymer layer, allowing for the calculation of the thin-film interference. The substrate thickness in both cases is assumed to be longer than the coherent length of the light source; therefore, the reflections from

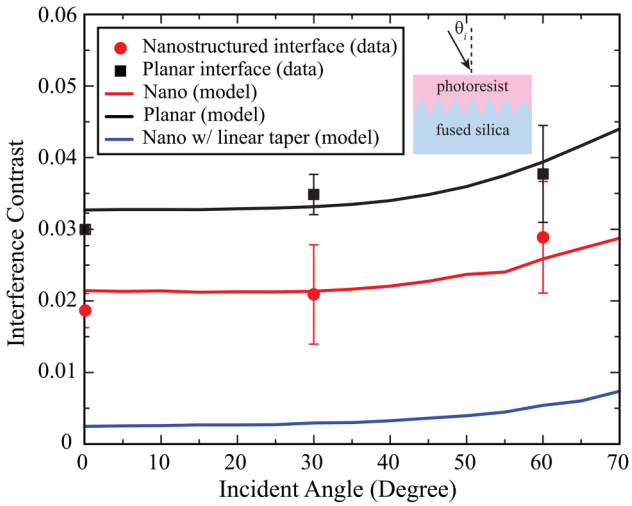

FIG. 6. Measured interference contrast for thin polymer film on fused silica substrates with nanostructured and planar interfaces. The simulations models for fabricated nanostructure, planar, and ideal linear taper are also shown.

the backside of the substrates do not interfere. The reflection efficiencies were modeled using Fresnel equations to account for the losses in the theoretical transmission. A third model with a linear taper profile was also included, demonstrating that further interference mitigation is possible with improved nanostructures profile.

The experimentally measured contrast data for both planar and nanostructured interfaces fit well to the simulation models. These results indicate that the interference contrast of the samples with interfacial nanostructures can be reduced roughly by a factor of two compared to those without. The suppression of interference effects can also be observed at both incident angles of 0° and 30°. The simulation result also shows that with improved nanostructures height and profile, the contrast can be reduced further by a factor of 10. These results indicate that interfacial nanostructures are effective in suppressing the interference effect, which can eliminate iridescent appearance and wavelength/angle-dependent transmission.

Going beyond the suppression of thin-film interference, the interfacial nanostructures can also improve light transmission for thick films. To demonstrate this, we first characterize the transmission of the double-side patterned silica substrate using a 633 nm HeNe laser (Model 30995, Research Electro-Optics, Inc.). A rotation stage was used to rotate the sample to change the incident angles from 0° to 70° with a 1° resolution. For incident angles larger than 70°, the illumination area exceeds the area of the nanostructures material and therefore is not considered. A photodiode detector (Model 918D-UV-OD3, Newport Co.) was used to measure the transmitted light intensity. The transmission for both TE and TM polarizations was characterized. The measured transmission and theoretical model of single fused silica substrate with and without double-side patterned nanostructures is plotted in Fig. 7. It can be observed that the data agree well with the RCWA and Fresnel models for the samples with and without the nanostructures, respectively. For TE polarization, the transmission is enhanced by ~5% near normal incidence, and up to 20% at 60°–70° incident angle range. For the maximum incident angle of 70°, the measured transmission for the sample with and without the nanostructures is 80% and 48%, respectively. However, the optical transmission of the nanostructured sample is lower for TM polarization between 50° and 70° incident angle ranges. This can be attributed to the Brewster angle effect, where the transmission for the planar sample is 100%. The nanostructured sample, in comparison, has scattering losses due to fabrication defects. Therefore, in this angle range, the defect losses are greater than the transmission gains due to the gradient-index matching effects, resulting in lower transmission for the nanostructured samples. The measurement error bar is within 1.5% based on multiple measurements.

The measured transmission and theoretical calculations for the thick 3-layer silica-polymer composite with and without the interfacial nanostructures are shown in Fig. 8. The sample was fabricated by bonding three double-side patterned fused silica substrates with two epoxy layers, as illustrated in the inset diagram. Note that in this case, the theoretical models assume no interference occurs since the layers are thick; therefore, the transmissions at the interfaces were simulated separately and multiplied together to yield the total transmission. It is important to note that if the thicknesses of the silica substrates and polymer layers are reduced so that they are sufficiently thin to result in an interference under ambient light, the interfacial nanostructures are also expected to suppress the interference effect. The experiment results show that under illumination TE polarized light, the transmission is enhanced by 7% at normal incidence, and up to 30% at 60°–70° incident angle ranges. For the maximum incident angle of 70°, the measured transmission for the composite with and without the nanostructures is 72% and 46%, respectively. For TM-polarized light, similar

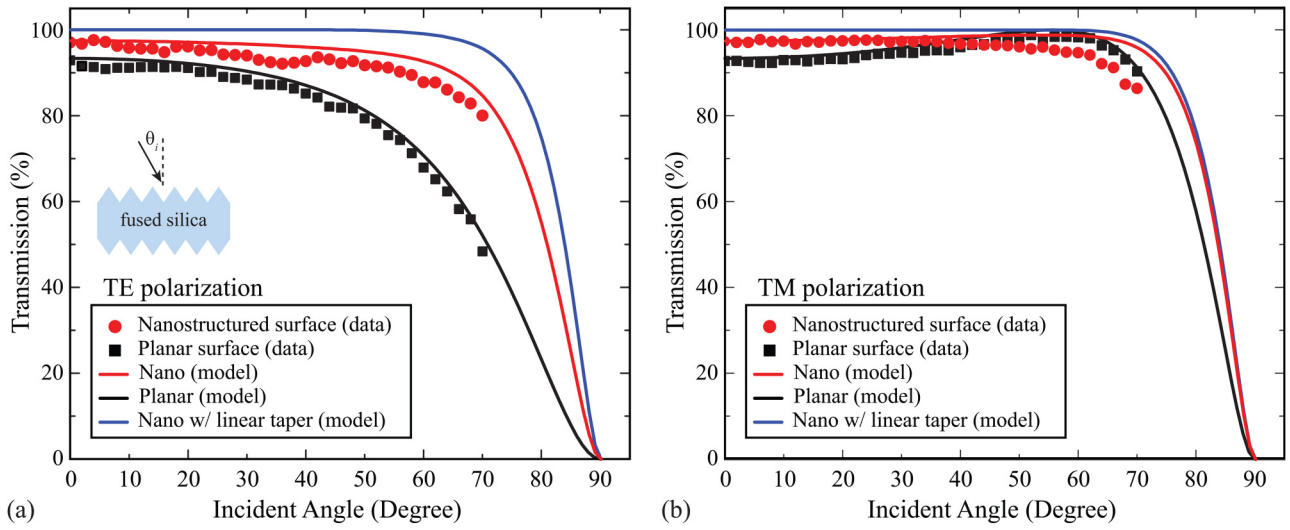

FIG. 7. Specular transmission measurement and simulation under different incident angles for fused silica substrate with and without double-side nanostructures for (a) TE and (b) TM polarization.

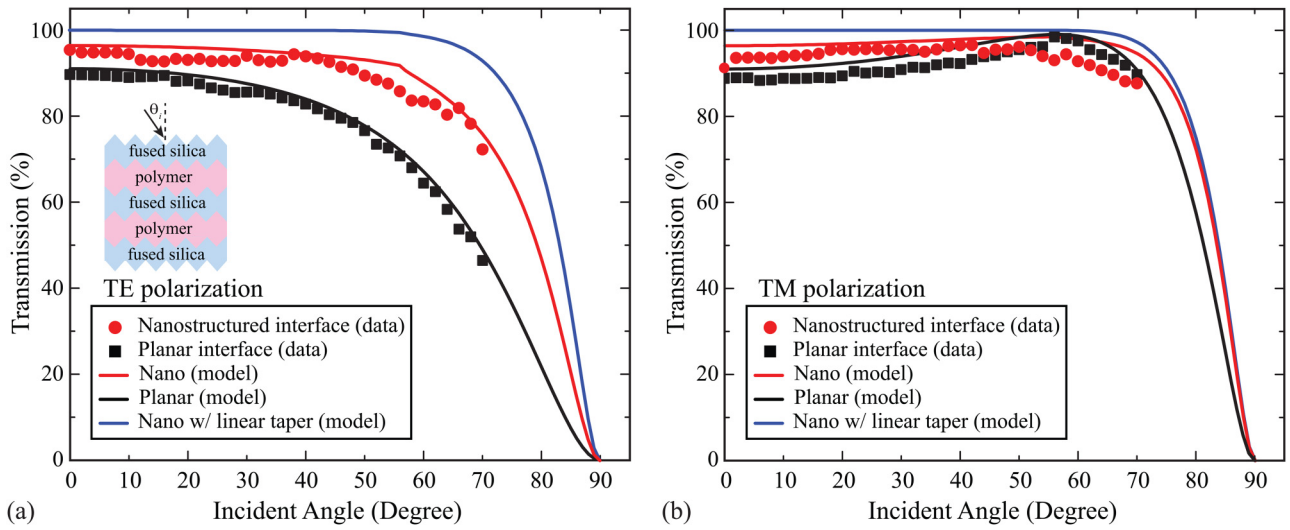

FIG. 8. Specular transmission measurement and simulation under different incident angles for a thick 3-layer silica-polymer multilayer composite with and without interfacial nanostructures for (a) TE and (b) TM polarization.

enhancement for the planar interface sample can be observed due to the Brewster angle, while the transmission for the nanostructured interface sample reduces monotonically at increasing incident angles. The measurement error bar based on the standard deviation of multiple measurements is within 1%. The simulation model also demonstrates that the near-perfect transmission can be maintained at highly oblique incident angles for taller interfacial nanostructures with a more effective tapper profile for both polarizations.

It is important to note that the transmission enhancement for 3 layers is not significant due to the relatively similar index of fused silica and epoxy used. However, the improvement would be significant at a higher number of layers (N). The theoretical transmission for 5, 10, and 20 layers with the planar and nanostructured interface is plotted in Fig. 9, which illustrates significant enhancement. The nanostructure is modeled to have 750 nm height with a linear taper profile. The transmission of the sample with planar interface

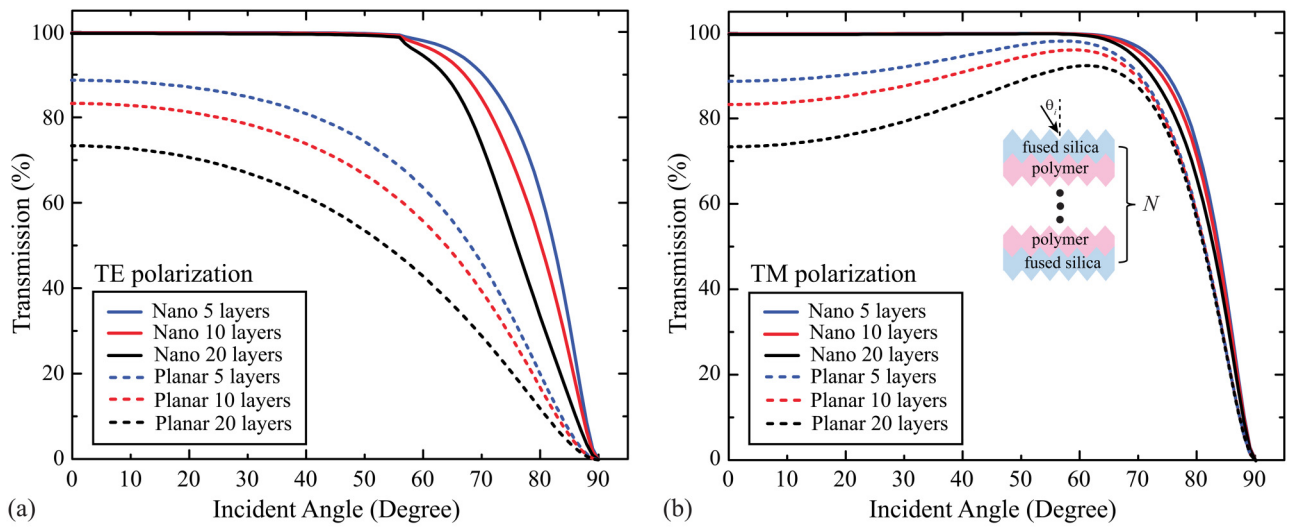

FIG. 9. Specular transmission simulation under different incident angles for 5, 10, and 20 layers thick silica-polymer composite with and without interfacial nanostructures for (a) TE and (b) TM polarization.

degrades significantly. However, the transmission can be maintained at near unity even at a high incident angle for the corresponding composite with interfacial nanostructures. These results demonstrate that the interfacial nanostructures are effective in suppressing the reflection at the multiple polymer-silica interfaces to enhance overall transmission. Enhancement in more number of layers would yield higher transmission enhancement and is the subject of ongoing research.

The broadband transmittance of the thick 3-layer silica-polymer composite with and without the nanostructures at the interfaces was also characterized at normal incidence and 30° incident angle, as shown in Figs. 10(a) and 10(b), respectively. Here, it can be observed that the transmission across a broad wavelength band can be enhanced. From Fig. 10(a), the measurement data illustrate that up to 7% enhancement can be observed at 450–800 nm wavelength, with a peak transmission of 97% compared with 90% without the nanostructures. The enhancement is reduced at a wavelength below 450 nm, and the transmission of the two samples is similar. This can be attributed to the relatively large structure period of 250 nm, which means diffracted orders in the UV can exist in the higher index polymer. The UV-curable epoxy also absorbs in the UV, therefore reducing transmission for both samples. From Fig. 10(b), we can observe that the transmission enhancement at 30° incident angle is up to 8%, with a peak transmission of 95% compared with 87% without the nanostructures. This is in reasonable agreement with the simulated models. Additional losses can be attributed to fabrication defects which have a larger footprint for off-axis illumination. The transmission data illustrate that the interfacial nanostructures work for broadband range and higher incident angle as predicted by the models. Note that the thickness of the fused silica and epoxy layers is approximately 0.5 mm and 0.1 mm, respectively, but some variations in the epoxy can occur during the bonding process. Due to the relative thick layers, thin-film interference effects are not observed. However, interference effects can still be present if the multilayer composites are under illumination from a light source with higher coherence.

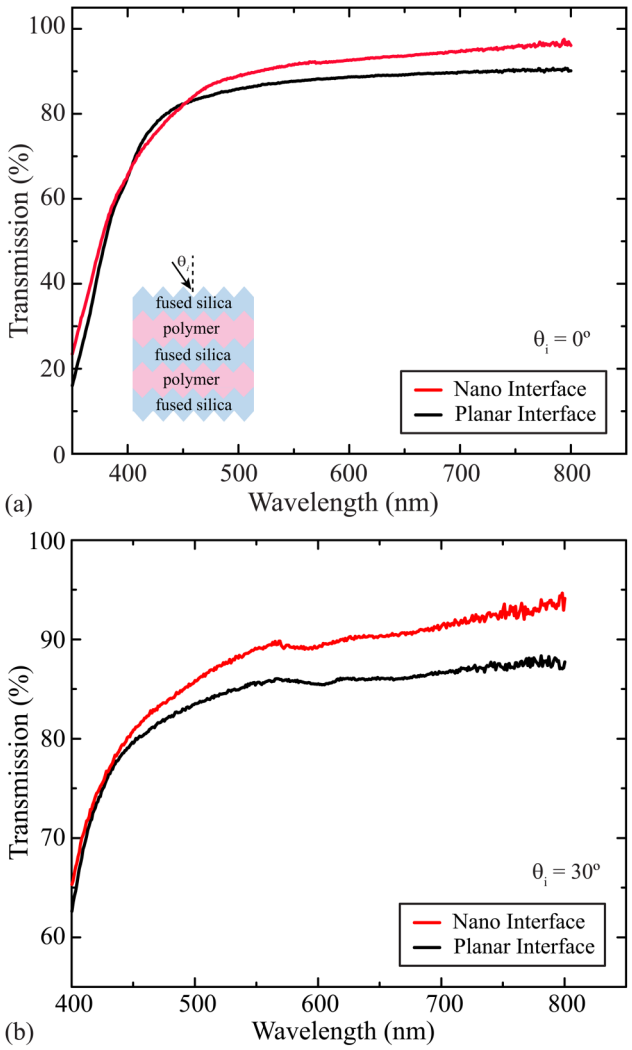

FIG. 10. Broadband specular transmittance measurements of a thick 3-layer silica-polymer multilayer composite with and without interfacial nanostructure at (a) 0° and (b) 30° incident angles.

These results and the derived models indicate that by using interfacial nanostructures, the reflection between two materials can be successfully suppressed. This effect, in turn, suppresses the interference in multilayer composites, allowing for wavelength and angle-independent optical behavior. For better interfacial antireflection effects than those demonstrated, taller structures[12] with an optimal taper profile can be used.[42,43] While the experimental data follow the trends predicted by the RCWA and Fresnel equation, errors can be observed. This can be attributed to the defects of the nanostructures. The proposed fabrication methods based on IL and RIE can be scalable, and full wafer patterning is possible. However, the defect areas from multiple samples can compound after bonding, resulting in scattering losses. We believe that this may lead to the transmission enhancement being slightly lower than theoretical models. However, the overall agreement between the data and theoretical model demonstrates that the interfacial nanostructure can enhance transmission of multilayer composite, which is the main focus of this study.

The experimental demonstration of this work is focused on the transmission enhancement between polymer and silica, which has relatively low reflection losses. The proposed interfacial nanostructures can even be more effective for higher index materials that are often used in optoelectronics, such as Si, Ge, and GaAs. Using the validated multilayer RCWA model, the transmission can be studied for a five-layer composite ($N = 5$) with higher index mismatch ($n_1 = 1.5$ and $n_2 = 3$) vs normalized interfacial nanostructure height and period, as shown in Fig. 11. Note that only the 0th-order specular transmission is considered, and any diffracted light is considered to be a loss. Here, it can be observed that the transmission of the composite with planar interfaces is 35.9% at normal incidence, corresponding to $H = 0$ in Fig. 11(a). The transmission can be enhanced to 94.4% for structure height $H = 0.6\lambda$ and period $\Lambda = 0.3\lambda$. Note that since the light wavelength in a higher index medium reduces, a smaller interfacial nanostructure

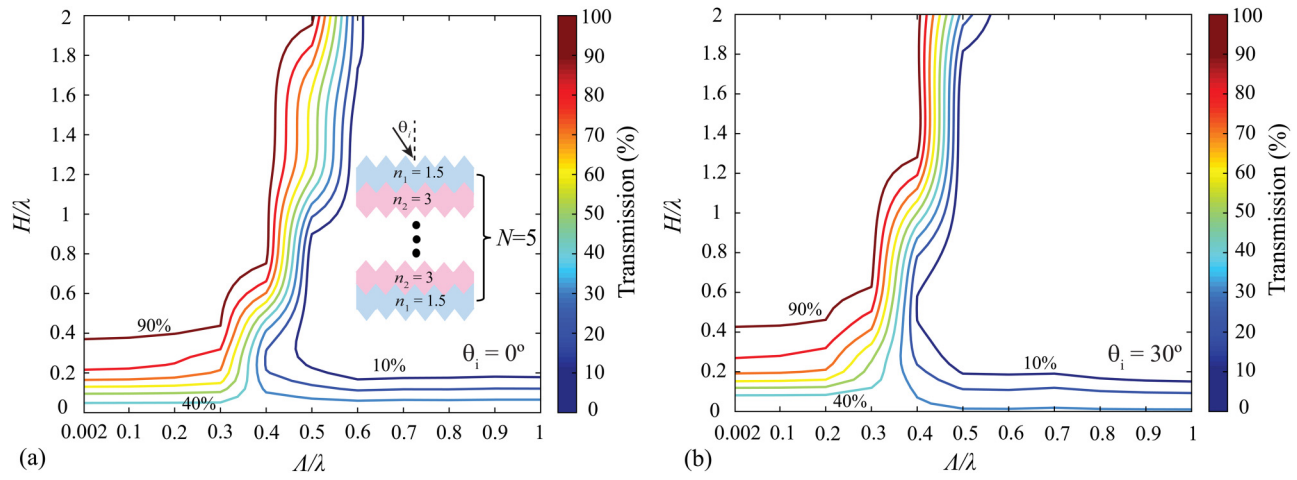

FIG. 11. Simulated 2D contour plots of specular transmission in 5-layer composite ($N = 5$) ($n_1 = 1.5$ and $n_2 = 3$). The transmission efficiency is plotted vs normalized structure height and period at incident angles of (a) $\theta_i = 0°$ and (b) $\theta_i = 30°$.

period is required to ensure subwavelength operation. As the structure height increases to $H = 2\lambda$ at the same period, the transmission can be further enhanced to 99.8%. At incident angle $\theta_i = 30°$, the transmission of planar sample is 30.6%, demonstrating higher losses. The transmission can be enhanced to 88.5% and 99.7% for structure heights of $H = 0.6\lambda$ and $H = 2\lambda$, respectively, both with period $\Lambda = 0.3\lambda$.

One interesting phenomenon that can be observed is that for structures with larger period, the transmission drops dramatically. This can be observed for any structures with constant H, where the transmission decreases as the period increases. This can be attributed to the diffraction effect for large period. This then shifts the efficiency of the 0th order, dramatically decreasing the specular transmission. From these results, it can be concluded that the period must be smaller than 0.3λ to ensure subwavelength operation. Note that this criterion is limited to this simulated case where the highest index is $n_2 = 3$ and can shift for multilayer systems with higher or lower indices. It is important to observe that reducing the period further does not result in any transmission enhancement and is only useful for lowering the operating wavelength range. In addition, higher nanostructures also result in better transmission enhancement for a constant period. However, the enhancement is incremental and may not justify the higher fabrication cost. These results demonstrate that interfacial nanostructures are an effective way to enhance transmission in composite with higher index mismatch, which can improve the performance of nanophotonic devices, solar cells, and solid-state lighting.

For future work, different mask materials will be used to fabricate taller interfacial nanostructures with height over 700 nm for better AR effects at a longer wavelength and higher incident angles. We will also investigate interfacial nanostructures with a shorter period less than 200 nm, which can reduce the diffraction and therefore improve the optical transmission in UV region. The profile of the structure will also be fine-tuned to obtain a wider range of tapered width. The yield will also be improved to reduce scattering losses and further enhance transmission. In addition, composite samples with more layers will be tested to demonstrate scalability and achieve higher transmission enhancement. The nanostructured interface can also have novel mechanical and thermal properties, which is the subject of ongoing research.

CONCLUSION

In this study, we investigate and demonstrate that interfacial nanostructures in multilayer composite stacks can reduce interfacial reflections, suppress interference effects, and enhance light transmission. This is supported by experimental characterization and theoretical modeling of light transmission in thin and thick multilayer films consisting of nanostructured interface between neighboring silica and polymer layers. The experimental data show that the interference contrast observed in the transmittance of thin films can be suppressed by a factor of two, and thick 3-layer silica-polymer composites can exhibit transmission enhancement up to 30% at 60°–70° incident angle range. From the experiment results, the enhancement is broadband and is effective at higher incident angle, and the fabricated interfacial nanostructures show higher transmission from 450–800 nm wavelength. The interfacial nanostructure can result in higher transmission enhancement for composites with higher refractive index mismatch, which has been studied using the validated RCWA models. This work demonstrated that interfacial nanostructures can reduce reflection losses in multilayers composites, increasing transmission and suppressing interference effects. This can mitigate wavelength and angle-dependence behaviors and enhance broadband transmission in multilayers photonic element and devices.

ACKNOWLEDGMENTS

This work was performed in part at the NCSU Nanofabrication Facility (NNF) and the Analytical Instrumentation Facility (AIF), members of the North Carolina Research Triangle Nanotechnology Network (RTNN), which is supported by the National Science

Foundation (NSF) as part of the National Nanotechnology Coordinated Infrastructure (NNCI). This work was supported by the Army Research Office (ARO) under Grant No. W911NF-16-1-0314 and partially supported by the National Science Foundation (NSF) under Grant No. CMMI#1552424.

REFERENCES

[1]P. B. Clapham and M. C. Hutley, "Reduction of lens reflexion by the 'moth eye' principle," Nature **244**, 281–282 (1973).
[2]S. J. Wilson and M. C. Hutley, "The optical properties of "moth eye" antireflection surfaces," Opt. Acta Int. J. Opt. **29**, 993–1009 (1982).
[3]D. H. Raguin and G. M. Morris, "Antireflection structured surfaces for the infrared spectral region," Appl. Opt. **32**, 1154–1167 (1993).
[4]P. Lalanne and G. M. Morris, "Antireflection behavior of silicon subwavelength periodic structures for visible light," Nanotechnology **8**, 53–56 (1997).
[5]Y. Kanamori, M. Sasaki, and K. Hane, "Broadband antireflection gratings fabricated upon silicon substrates," Opt. Lett. **24**, 1422–1424 (1999).
[6]P. Vukusic and J. R. Sambles, "Photonic structures in biology," Nature **424**, 852–855 (2003).
[7]D. G. Stavenga, S. Foletti, G. Palasantzas, and K. Arikawa, "Light on the moth-eye corneal nipple array of butterflies," Proc. R. Soc. Lond. B Biol. Sci. **273**, 661–667 (2006).
[8]A. R. Parker and H. E. Townley, "Biomimetics of photonic nanostructures," Nat. Nanotechnol. **2**, 347–353 (2007).
[9]S. A. Boden and D. M. Bagnall, "Tunable reflection minima of nanostructured antireflective surfaces," Appl. Phys. Lett. **93**, 133108 (2008).
[10]J.-Q. Xi, M. F. Schubert, J. K. Kim, E. F. Schubert, M. Chen, S.-Y. Lin, W. Liu, and J. A. Smart, "Optical thin-film materials with low refractive index for broadband elimination of Fresnel reflection," Nat. Photonics **1**, 176–179 (2007).
[11]Y. M. Song, S. J. Jang, J. S. Yu, and Y. T. Lee, "Bioinspired parabola subwavelength structures for improved broadband antireflection," Small **6**, 984–987 (2010).
[12]K.-C. Park, H. J. Choi, C.-H. Chang, R. E. Cohen, G. H. McKinley, and G. Barbastathis, "Nanotextured silica surfaces with robust superhydrophobicity and omnidirectional broadband supertransmissivity," ACS Nano **6**, 3789–3799 (2012).
[13]X. Ye, X. Jiang, J. Huang, F. Geng, L. Sun, X. Zu, W. Wu, and W. Zheng, "Formation of broadband antireflective and superhydrophilic subwavelength structures on fused silica using one-step self-masking reactive ion etching," Sci. Rep. **5**, 13023 (2015).
[14]Z. Diao, M. Kraus, R. Brunner, J.-H. Dirks, and J. P. Spatz, "Nanostructured stealth surfaces for visible and near-infrared light," Nano Lett. **16**, 6610–6616 (2016).
[15]H. Wang, H. Qi, B. Wang, Y. Cui, Y. Chai, Y. Jin, K. Yi, and J. Shao, "Near-field enhancement of the nanostructure on the fused silica with rigorous method," Appl. Opt. **54**, 4318–4326 (2015).
[16]S. Chattopadhyay, Y. F. Huang, Y. J. Jen, A. Ganguly, K. H. Chen, and L. C. Chen, "Anti-reflecting and photonic nanostructures," Mater. Sci. Eng. R Rep. **69**, 1–35 (2010).
[17]W. H. Southwell, "Pyramid-array surface-relief structures producing antireflection index matching on optical surfaces," J. Opt. Soc. Am. A **8**, 549–553 (1991).
[18]D. Poitras and J. A. Dobrowolski, "Toward perfect antireflection coatings. 2. Theory," Appl. Opt. **43**, 1286–1295 (2004).
[19]M. Zubair, Y. S. Ang, K. J. A. Ooi, and L. K. Ang, "Fractional Fresnel coefficients for optical absorption in femtosecond laser-induced rough metal surfaces," J. Appl. Phys. **124**, 163101 (2018).
[20]A. Bagal, X. A. Zhang, R. Shahrin, E. C. Dandley, J. Zhao, F. R. Poblete, C. J. Oldham, Y. Zhu, G. N. Parsons, C. Bobko, and C.-H. Chang, "Large-area nanolattice film with enhanced modulus, hardness, and energy dissipation," Sci. Rep. **7**, 9145 (2017).
[21]C.-H. Sun, P. Jiang, and B. Jiang, "Broadband moth-eye antireflection coatings on silicon," Appl. Phys. Lett. **92**, 061112 (2008).
[22]H. Park, D. Shin, G. Kang, S. Baek, K. Kim, and W. J. Padilla, "Broadband optical antireflection enhancement by integrating antireflective nanoislands with silicon nanoconical-frustum arrays," Adv. Mater. **23**, 5796–5800 (2011).
[23]Y.-F. Huang, S. Chattopadhyay, Y.-J. Jen, C.-Y. Peng, T.-A. Liu, Y.-K. Hsu, C.-L. Pan, H.-C. Lo, C.-H. Hsu, Y.-H. Chang, C.-S. Lee, K.-H. Chen, and L.-C. Chen, "Improved broadband and quasi-omnidirectional anti-reflection properties with biomimetic silicon nanostructures," Nat. Nanotechnol. **2**, 770–774 (2007).
[24]A. H. Peltier, G. Sapkota, J. R. Case, and M. K. Poutous, "Polarization insensitive performance of randomly structured antireflecting planar surfaces," Opt. Eng. **57**, 037109 (2018).
[25]M.-L. Kuo, D. J. Poxson, Y. S. Kim, F. W. Mont, J. K. Kim, E. F. Schubert, and S.-Y. Lin, "Realization of a near-perfect antireflection coating for silicon solar energy utilization," Opt. Lett. **33**, 2527–2529 (2008).
[26]X. A. Zhang, Y.-A. Chen, A. Bagal, and C.-H. Chang, "Enhanced total internal reflection using low-index nanolattice materials," Opt. Lett. **42**, 4123–4126 (2017).
[27]Q. Xu, V. R. Almeida, R. R. Panepucci, and M. Lipson, "Experimental demonstration of guiding and confining light in nanometer-size low-refractive-index material," Opt. Lett. **29**, 1626–1628 (2004).
[28]J. K. Kim, T. Gessmann, E. F. Schubert, J.-Q. Xi, H. Luo, J. Cho, C. Sone, and Y. Park, "GaInN light-emitting diode with conductive omnidirectional reflector having a low-refractive-index indium-tin oxide layer," Appl. Phys. Lett. **88**, 013501 (2006).
[29]J. Zhu, C.-M. Hsu, Z. Yu, S. Fan, and Y. Cui, "Nanodome solar cells with efficient light management and self-cleaning," Nano Lett. **10**, 1979–1984 (2009).
[30]K. X. Wang, Z. Yu, V. Liu, Y. Cui, and S. Fan, "Absorption enhancement in ultrathin crystalline silicon solar cells with antireflection and light-trapping nanocone gratings," Nano Lett. **12**, 1616–1619 (2012).
[31]M. G. Deceglie, V. E. Ferry, A. P. Alivisatos, and H. A. Atwater, "Design of nanostructured solar cells using coupled optical and electrical modeling," Nano Lett. **12**, 2894–2900 (2012).
[32]J. Tippens, A. Bagal, X. A. Zhang, and C.-H. Chang, "Nanostructured antireflective in-plane solar harvester," Opt. Express **25**, A840–A850 (2017).
[33]P. Pignalosa, B. Liu, H. Chen, H. Smith, and Y. Yi, "Giant light extraction enhancement of medical imaging scintillation materials using biologically inspired integrated nanostructures," Opt. Lett. **37**, 2808–2810 (2012).
[34]A. P. Jackson, F. V. Vincent Julian, R. M. Turner, and A. R. Mcneill, "The mechanical design of nacre," Proc. R. Soc. Lond. B Biol. Sci. **234**, 415–440 (1988).
[35]R. Z. Wang, Z. Suo, A. G. Evans, N. Yao, and I. A. Aksay, "Deformation mechanisms in nacre," J. Mater. Res. **16**, 2485–2493 (2001).
[36]X. Li, W.-C. Chang, Y. J. Chao, R. Wang, and M. Chang, "Nanoscale structural and mechanical characterization of a natural nanocomposite material: The shell of Red abalone," Nano Lett. **4**, 613–617 (2004).
[37]F. Barthelat, C.-M. Li, C. Comi, and H. D. Espinosa, "Mechanical properties of nacre constituents and their impact on mechanical performance," J. Mater. Res. **21**, 1977–1986 (2006).
[38]Q. Yang, X. A. Zhang, A. Bagal, W. Guo, and C.-H. Chang, "Antireflection effects at nanostructured material interfaces and the suppression of thin-film interference," Nanotechnology **24**, 235202 (2013).
[39]M. G. Moharam, E. B. Grann, D. A. Pommet, and T. K. Gaylord, "Formulation for stable and efficient implementation of the rigorous coupled-wave analysis of binary gratings," J. Opt. Soc. Am. A **12**, 1068–1076 (1995).
[40]M. G. Moharam, D. A. Pommet, E. B. Grann, and T. K. Gaylord, "Stable implementation of the rigorous coupled-wave analysis for surface-relief gratings: Enhanced transmittance matrix approach," J. Opt. Soc. Am. A **12**, 1077–1086 (1995).
[41]H. I. Smith, "Low cost nanolithography with nanoaccuracy," Phys. E Low-Dimens. Syst. Nanostruct. **11**, 104–109 (2001).
[42]E. B. Grann, M. G. Moharam, and D. A. Pommet, "Optimal design for antireflective tapered two-dimensional subwavelength grating structures," J. Opt. Soc. Am. A **12**, 333–339 (1995).
[43]Y. Zhang, C. Li, and M. Loncar, "Optimal broadband antireflective taper," Opt. Lett. **38**, 646–648 (2013).